Journal of the European Ceramic Society 39 (2019) 2731–2738

Contents lists available at ScienceDirect

Journal of the European Ceramic Society

journal homepage: www.elsevier.com/locate/jeurceramsoc

Original Article

3D printed ceramic phosphor and the photoluminescence property under blue laser excitation

Song Hu[a,b,c], Yingli Liu[a,c], Yunli Zhang[a,c], Zhenhai Xue[a,c], Zhengjuan Wang[a,b,c], Guohong Zhou[a,b,c,*], Chunhua Lu[d], Hongshu Li[e], Shiwei Wang[a,c,*]

[a] State Key Laboratory of High Performance Ceramics and Superfine Microstructure, Shanghai Institute of Ceramics, Chinese Academy of Sciences, Shanghai 200050, China
[b] Center of Materials Science and Optoelectronics Engineering, University of Chinese Academy of Sciences, Beijing 100049, China
[c] Key Laboratory of Transparent Opto-functional Inorganic Materials, Shanghai Institute of Ceramics, Chinese Academy of Sciences, Shanghai 210899, China
[d] Nanjing Tech University, Nanjing 210009, China
[e] Shanghai Meipai Industrial Co., Ltd, Shanghai 201907, China

ARTICLE INFO

Keywords:
3D printing
Dimensional accuracy
Ceramic phosphor
High-flux laser lighting
Microstructure

ABSTRACT

An Al_2O_3/YAG: Ce^{3+} ceramic phosphor was fabricated for high-flux laser lighting using the digital lighting process (DLP)-based 3D printing method for the first time. The photocurable ceramic suspension for 3D printing was prepared by blending well-treated Al_2O_3/YAG: Ce^{3+} composite powders with photosensitive resin monomers and photo-initiators. The printing parameters, debinding and sintering processes were designed delicately to fabricated the dense sub-millimeter-sized cylinder ceramic with high dimensional accuracy. The ceramic showed excellent luminescence property under blue laser excitation with a threshold of 20.7 W/mm^2, higher than that prepared via dry-pressing followed by vacuum sintering. The luminescence properties and the microstructures of both ceramics were further comparatively investigated to find the possible interpretations for improvement of laser flux for the 3D-printed ceramic. The present work indicated that the new developed 3D printing method was promising for preparing luminescent ceramics for high-flux laser lighting in a rapid, effective, low-cost and precision-controlled manner.

1. Introduction

Ceramic phosphors are emerging as preferences in special lighting technologies, especially the laser diode (LD)-based lighting with high power density, due to their excellent thermal endurance property and the thermal stability of luminescence compared with those of the resin encapsulated phosphors or the phosphor in glasses (PiGs) [1–4]. After several years' research and development, the garnet-structured ceramics, such as YAG, LuAG ceramics, have been standing out from the mostly studied ones, benefiting from their excellent optical as well as thermal-stability properties [5,6]. In recent, a new type of Al_2O_3/YAG: Ce^{3+} composite ceramics containing homogeneously distributed Al_2O_3 grains called "scattering centers" in YAG: Ce^{3+} ceramic matrix have drawn much attention for the remarkable enhanced light extraction efficiency and effective thermal conductivity [7–10]. The commonly used manufacturing methods for those ceramic phosphors such as dry-pressing [11], tap-casting [12], and gel-casting [13] are proved mature and favorable to obtain ceramics with excellent luminescent performance, however, not efficient or economical enough. For instance, subjected to the forming technology, the finally obtained ceramics have to be polished to remove impurities (e.g., graphite) on double-surfaces, lapped to reach desired thickness and incised to the designed shapes or geometric configurations before they can be encapsulated onto optical modules. Moreover, the mentioned forming technologies may be confronted with inconveniences that complex instrument systems such as high-pressure or high-voltage systems, costly procedures including cold-isostatic pressing, or easily consumable molds such as graphite molds or boron nitride coated carbon molds should be partially or simultaneously imported [14–16]. Thus, the complex procedure would inevitably lead to an increase of production cycle and the cost. Meanwhile, leftover materials would take up much costing once final products with complicated configurations are needed. To be noticed, for LD-based lighting, a ceramic with ultra-small and thin features are generally preferred as it can be used as a quasi-point source [4]. In this

* Corresponding authors at: State Key Laboratory of High Performance Ceramics and Superfine Microstructure, Shanghai Institute of Ceramics, Chinese Academy of Sciences, Shanghai 200050, China.
E-mail addresses: sic_ghzhou@mail.sic.ac.cn (G. Zhou), swwang51@mail.sic.ac.cn (S. Wang).

https://doi.org/10.1016/j.jeurceramsoc.2019.03.005
Received 15 January 2019; Received in revised form 26 February 2019; Accepted 1 March 2019
Available online 06 March 2019
0955-2219/

circumstance, a new forming strategy should be involved to prepare ceramics with small and precise dimensions more efficiently.

Three-dimensional (3D) printing is a new emerging technology creating ceramics by adding materials to form components with complex geometries according to computer-added designs (CAD) with almost no waste of raw materials while reaching satisfactory geometric accuracy [17], which have been actively developed in preparing ceramics including structural ceramics [18], ceramic-matrix composites [19], bio-active ceramics [20,21], and other functional ceramics, e.g., SiBCN ceramics with high thermal stability and excellent oxidation resistance [22]. G. A. Dosovitskiy [23] firstly reported a ceramic scintillator with complex configuration using 3D printing method. The ceramics exhibited challenging scintillation characteristics which can be largely ascribed from the well-designed geometries. However, the dimensional accuracy which was generally recognized as the other superiority of 3D printing was not demonstrated. More importantly, to our best knowledge, almost no further attentions have been paid to prepare the luminescent ceramics for laser lighting via 3D printing method, probably due to the not easily regulated defects in ceramics during forming and sintering, but the extreme demands for ceramics to sustain the laser irradiation with high power density.

In the present work, a 3D printing strategy was adopted to prepare the Al_2O_3/YAG: Ce^{3+} ceramic phosphor based on our previous study [8]. The dimensional characteristics were precisely controlled via regulating the photocurable resins, the composition of ceramic suspensions along with the printing parameters. The luminescence property under laser irradiations and the microstructure of the ceramic phosphor were emphatically elaborated and compared with those of the ceramic prepared via the traditional dry-pressing forming method.

2. Experimental procedures

An $Al_2O_3/Y_3Al_5O_{12}$: Ce^{3+} (Al_2O_3/YAG: Ce^{3+}) composite ceramic was firstly prepared via the high-end digital lighting processing (DLP) 3D printing technology. In the composite material, 0.4 mol.% Ce^{3+} ions were introduced to replace the corresponding Y^{3+} sites and the additional Al_2O_3 grains with a volume fraction of 22% acted as the scattering centers to enhance light extraction [8]. The preparation process was schematically presented in Fig. 1. Firstly, the composite powders composed of Al_2O_3, Y_2O_3, CeO_2, and a small fraction of sintering additives (TEOS and MgO) were weighed stoichiometrically and mixed thoroughly by ball-milling in ethanol. The slurry was dried at 60℃, grounded and sieved through a 200-mesh screen, followed by calcining at 900℃ for 2 h to obtain homogenously distributed sub-micron-sized powder mixture. Secondly, a suspension suitable for 3D printing was prepared by mixing the mixture with the commercial photocurable resins purchased from Ausbond Co., Ltd. (Shenzhen, China) and a small amount of hexanediol diacrylate. The suspension with a mass fraction of 77.8% for the powder mixture was finally obtained by further milling for 12 h for more uniform distribution. Thirdly, the DLP 3D printing procedure was conducted to create the Al_2O_3/YAG: Ce^{3+} green bodies from the computer-aided design (CAD) model with a lateral resolution of 10 μm and layer thickness of 30 μm, using the 3D printing technology development by ADMATEC Europe BV, the Netherlands. The debinding process was then carried out in several temperature stages according to the decomposing temperatures of the polymers as well as the TG/DSC curves. The dense ceramics with excellent performance were obtained after a further high temperature (1720℃) sintering process under vacuum and an annealing process were conducted. The ceramic was simply processed into slices with a thickness of 0.2 mm for diverse characterizations. For luminescence property comparison, a dry-pressing and vacuum sintering method was also applied to fabricate the Al_2O_3/YAG: Ce^{3+} composite ceramic, using the same Al_2O_3/YAG: Ce^{3+} powder as mentioned above. The forming and sintering processes followed our previous work [8]. A line cutting procedure was processed to divide the pellets into slices with the same thickness as that of the 3D-printed sample. Then laser beam cutting was adopted to incise the thin ceramics to get desired configurations.

The thermogravimetry (TG) and differential scanning calorimetry measurements of the green body were made using an STA449C analyzer, NETZSCH, Germany at a heating rate of 10 ℃/min in air. Phase composition of the final composite ceramic was characterized in the 2θ range from 10° to 80° with a step of 0.02°, using the micro-region X-ray diffraction (XRD) on a Bruker D8 Discover diffractometer with Cu Kα radiation (λ = 1.54056 Å). Scanning electron microscopy (SEM, Hitachi S-4800, Japan) equipped with an energy dispersive X-ray spectroscope (EDS, Oxford X-MaxN 80, Cambridge, UK) was used to observe the microstructure and confirm the composition of the ceramic. Therein, the backscattered electron (BSE) mode was used to visualize the thermal-etched surface and fracture surface of the prepared ceramic for better distinguishing the distribution of different polycrystals in the ceramic. The ceramic was then encapsulated on a heat sink for the laser activated photoluminescence evaluation. The luminescence spectra and the light yield were recorded on a home-made instrument containing a 455 nm laser, an integrating sphere, fiber sensors and the computer system. The micro-lenses were used to confine the spotlight of the laser beam.

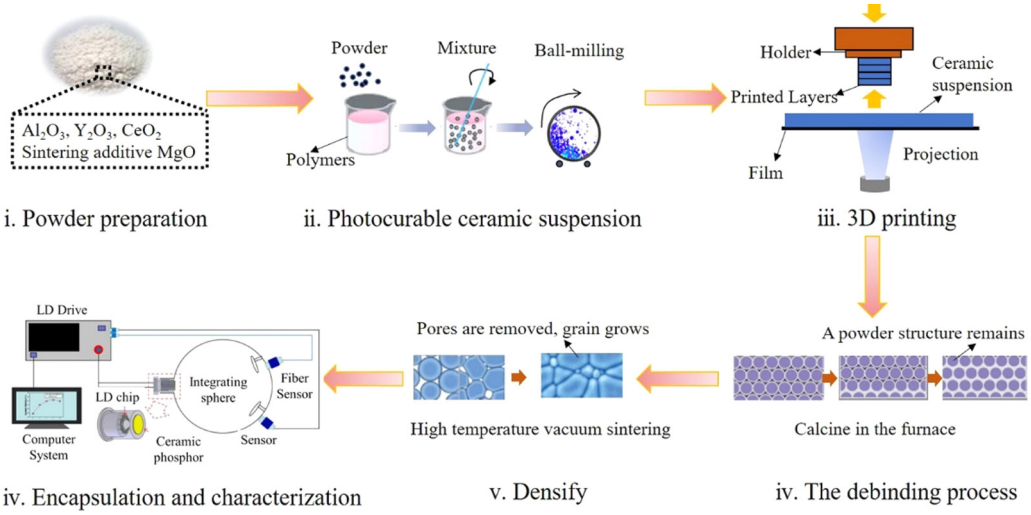

Fig. 1. The schematic diagram of the procedure for the preparation of the Al_2O_3/YAG: Ce^{3+} composite ceramic phosphor via 3D printing.

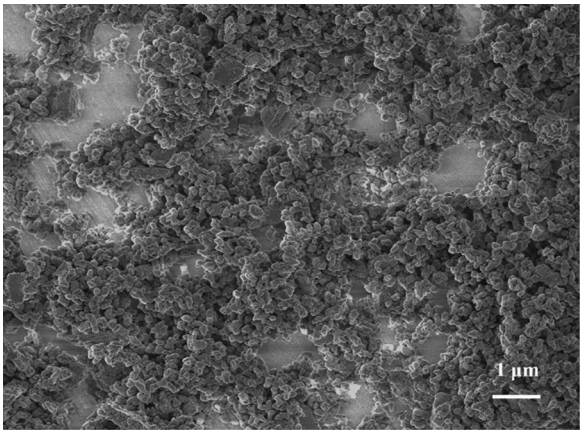

Fig. 2. Scanning electron microscopy (SEM) photograph of the powder mixture calcined at 800 ℃ for 3 h.

3. Results and discussion

Our strategy for preparing the Al_2O_3/YAG: Ce^{3+} composite ceramic with sub-millimeter features (900 μm in diameter, 5 cm in length) via the DLP based 3D printing has been elaborately depicted (Fig. 1) and proved efficient and exquisite, especially for those functional materials with complex shapes, ultra-small sizes or hierarchical structures. The powder mixture of Al_2O_3/YAG: Ce^{3+} was firstly carefully prepared through ball-milling, grinding, sieving, and pre-sintering, in order to prevent severe agglomeration and keep good flowability. Morphology of the prepared Al_2O_3/YAG: Ce^{3+} powder mixture was shown in Fig. 2, from which one can find that the powder mixture was dispersed homogenously with less agglomeration. This may confirm a high-density green body with less cracks or other defects [24].

DLP 3D printing is a layer-by-layer assembly technique upon which the photocurable ceramic suspension rapidly solidify selectively via gelation with the assistance of 405 nm light source and the DLP project [25,26]. The exposure time/intensity parameters are adjusted to satisfy the photopolymerization ability of the resin system and determine thickness of each cured layer. In the present study, the exposure parameters were carefully designed, as shown in Fig. 3(a), the boundaries between each layer were distinguishable, the thickness could be evaluated to be 30 μm. Due to the limitation of the bonding strength, defects still existed on the interlaminations. Fortunately, the interactions of each layer were strengthened as soon as the green bodies were cured carefully under relatively high temperature of 1000℃, as shown in Fig. 3(b). During heat-treatment, most of the polymers were decomposed, leaving the ceramic particles to stack freely firstly and followed by a densifying process due to the driving force of high temperature. As a result, the boundaries became blurring, and most defects were eliminating gravitationally. The heat-treatment process should be deliberated to avoid delamination, crack, deformation or warping. These phenomena occurred occasionally due to the high mass fraction of the

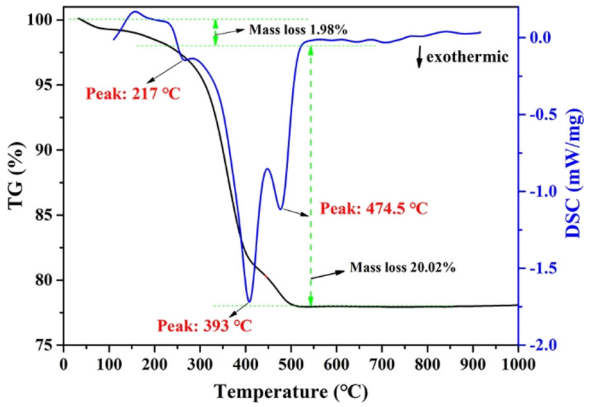

Fig. 4. TG-DSC curves of the printed green body of Al_2O_3/YAG: Ce^{3+} (heating rate, 10 ℃/min).

polymers (22 wt.%) which should be removed from the interspace between ceramic particles. Thus, the calcination temperature and the heating rate were well designed to provide sufficient time for polymerization and evaporation. The TG-DSC curves were recorded to determine the heat-treatment procedure, as presented in Fig. 4. Heating (heating rate, 10 ℃·min^{-1}) and pyrolysis led to a mass loss, registered by TG. The mass change of the printed preceramic occurred steadily from room temperature to 500℃, mainly in two steps, corresponding to different decomposition processes. The first step occurred below 230 ℃ with a weight loss of 1.98%, which might be ascribed to the evaporation of oligomers with low molecular weight. The second step happened in the temperature range from 230 to 520 ℃ with a total weight loss of 20.02%, during which the organic moiety and the crosslinked acrylate in the preceramic could decompose thoroughly. Above 520 ℃, the mass change was milder, indicating the conversion from polymer solidified preceramic to ceramic was almost completed. The residual weight for the ceramic was 78%, which was consistent with the component of the ceramic suspension with a mass fraction of 77.8%. The ceramic yield of the present study is much higher compared to the photocurable preceramic reported in the previous researches on oxide ceramics [23], which would contribute to the densification of the ceramic. During the second mass loss stage, three exothermic peaks at around 217, 393, and 474.5℃ could be found obviously, registered by DSC. These thermal effects probably corresponded to pyrolysis of the crosslinked polymers. As the polymers were decomposed thoroughly, the rearrangement of the ceramic particles occurred and the ceramic started to shrink and densify. Due to the precise control of the heating rate at different temperature regions, almost no cracks were found in the bisque ceramic.

For the purpose of providing the ceramic bisque with enough mechanical strength, the pre-sintering temperature was set up to 1000 ℃. After that, the ceramic bisque was transferred into a tungsten furnace and further sintered at 1720 ℃ for 3 h in vacuum. Fig. 5 shows the XRD pattern of the Al_2O_3/YAG:Ce^{3+} ceramic prepared via 3D printing

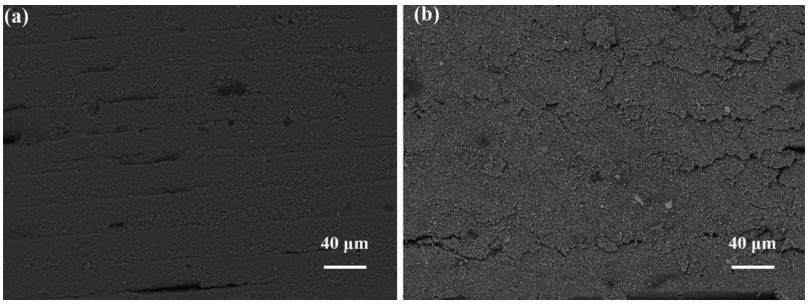

Fig. 3. SEM images of (a) the printed green body and (b) the bisque of Al_2O_3/YAG: Ce^{3+} treated at 1000℃ for 2 h.

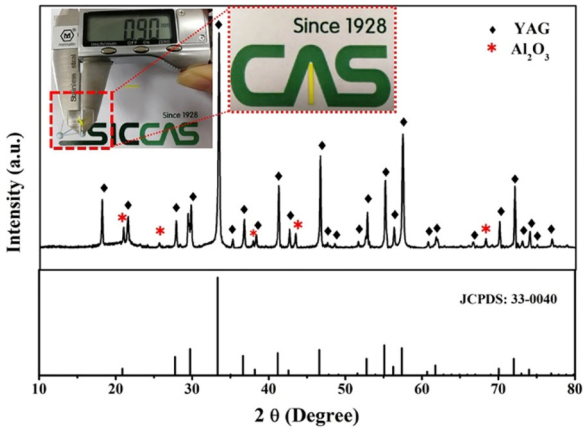

Fig. 5. XRD pattern of the 3D printed Al_2O_3/YAG:Ce^{3+} ceramic. Inset shows the appearance of the ceramic with fine dimensions.

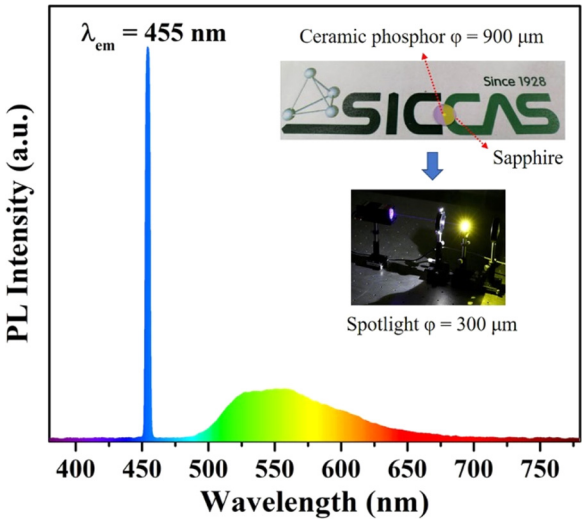

Fig. 7. Photoluminescence emission spectrum of the 3D printed Al_2O_3/YAG:Ce^{3+} ceramic. Inset shows the configuration of the simple module that ceramic was adhered onto the sapphire substrate (upper) and the illumined image with laser irradiation (below).

followed by vacuum sintering, indicating the existence of the second phase - Al_2O_3 in YAG (JCPDS: 33-0040) matrix. The Al_2O_3 crystals have been verified to be scattering centers for luminous efficiency increase [7,8,27,28], as well as beneficial medium for enhancing the effective thermal conductivity [4,10,29]. The inset shows the photograph of the Al_2O_3/YAG:Ce^{3+} ceramic with small diameter of 900 μm which was prepared as designed and no post-processing was conducted apart from incising into slices, indicating that the dimensional accuracy can be ensured using the present ceramic suspensions and the 3D printing parameters. It also demonstrates the virtually unlimited possibilities of 3D printing technology.

The cylinder ceramic was incised into slices with a thickness of 0.2 mm by single wire cutting and then thermal-etched at 1500 ℃ in air before laser activated photoluminescence evaluation. The microstructure of the composite ceramic was observed by SEM and the phase composition was indicated by EDS. Fig. 6(a) showed the surface of the ceramic, in which crystal grains with two distinguishable contrasts were confirmed to be YAG: Ce^{3+} (spectrum 1#) and Al_2O_3 (spectrum 2#) by EDS spectra in Fig. 6(c) and (d), respectively, which was consistent with the XRD result. The crystal grains of YAG were homogeneous with a mean size of 3~5 μm, no abnormally grown grains could be found in Fig. 6(a). Al_2O_3 grains were randomly dispersed among YAG crystal grains, whose crystal sizes were about 1~2 μm, slightly smaller than those of YAG, indicating that the powder mixture could be kept uniform and steady in the polymer containing suspension. Furthermore, from the side view (cross-section) of the ceramic shown in Fig. 6(b), one could also deduce that the side surface was smooth and the dimensional precision was well controlled. More importantly, the ceramic was dense enough that no pores were found in the grains or on the grain boundaries. This was attributed to the optimized components of the ceramic suspension, well-designed 3D printing parameters and properly regulated de-binding and sintering procedures. It also should be noted that no cracks could be found from both the surface and the

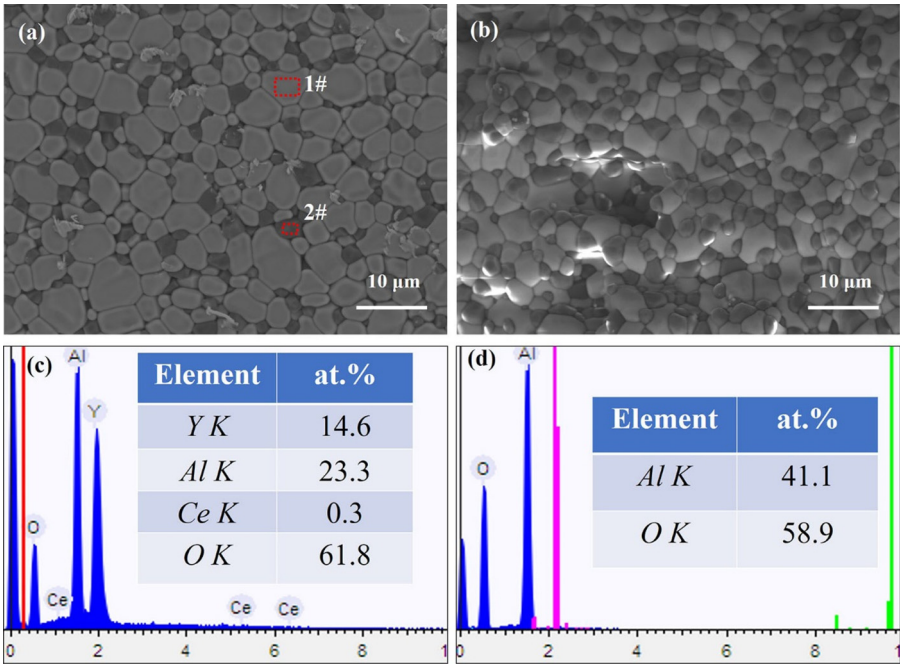

Element	at.%
Y K	14.6
Al K	23.3
Ce K	0.3
O K	61.8

Element	at.%
Al K	41.1
O K	58.9

Fig. 6. (a) BEI of the thermal-etched surface of the Al_2O_3/YAG: Ce^{3+} ceramic and the scanning sites labeled by Spectrum 1and 2; (b) BEI from the side view of the columnar ceramic; (c) and (d) are EDS analysis of spectrum 1 and spectrum 2, respectively.

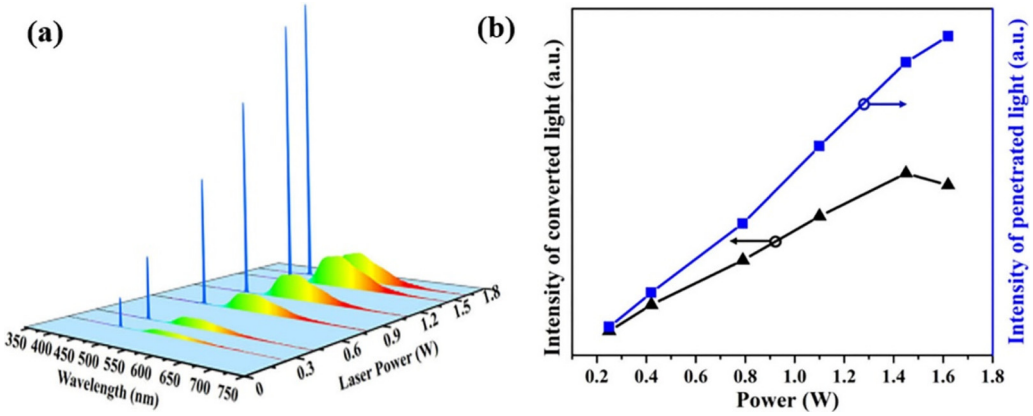

Fig. 8. (a) Spectra of the penetrated excitation laser light and the luminescence from the Al_2O_3/YAG: Ce^{3+} ceramic prepared via 3D printing; (b) intensities of both the penetrated light and the converted light as a function of pumping power.

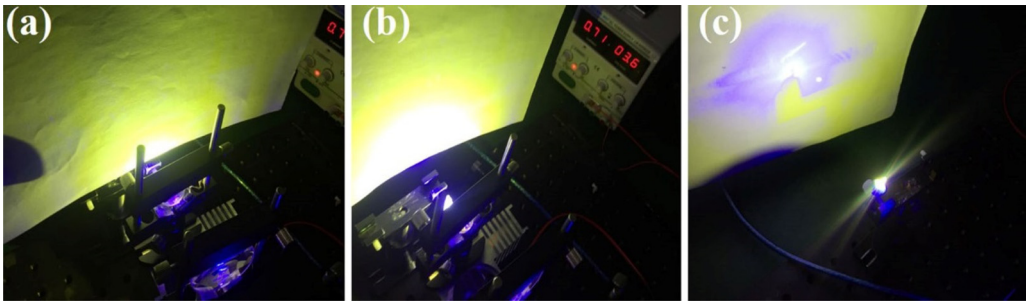

Fig. 9. Photographs of the emission light from Al_2O_3/YAG: Ce^{3+} ceramic prepared via 3D printing, under different excitation laser powers. (a) 0.25 W; (b) 1.45 W; (c) 1.62 W.

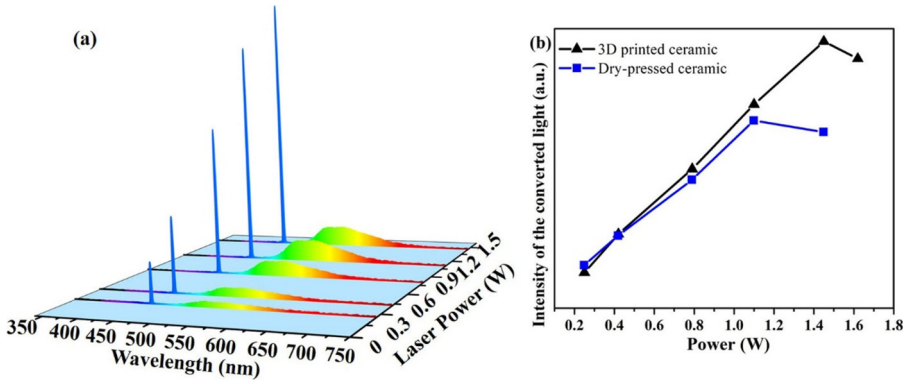

Fig. 10. (a) Spectra of the penetrated excitation laser light and the luminescence from the Al_2O_3/YAG: Ce^{3+} ceramic prepared via dry-pressing; (b) the plots of the emission intensity versus the excitation power for the ceramic-phosphors prepared via 3D printing and dry-pressing method.

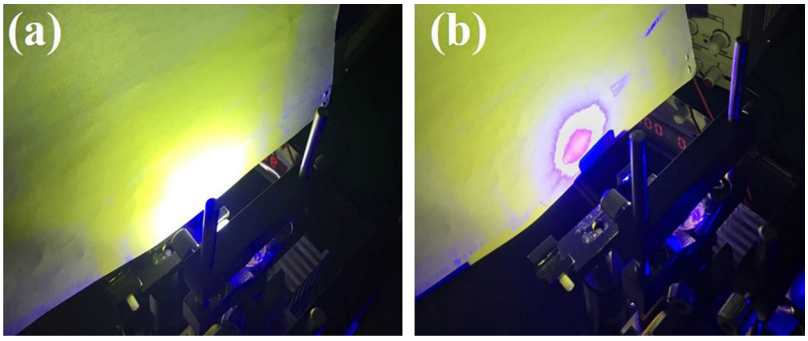

Fig. 11. Photographs of the emission light from Al_2O_3/YAG: Ce^{3+} ceramic prepared via dry-pressing, under different excitation laser powers. (a) 1.1 W; (b) 1.45 W.

Table 1
The color coordinates for both dry-pressed and 3D-printed ceramics under laser irradiation with increasing laser power density.

Laser Power (W)	Color coordinates (x, y)	
	3D-printed ceramic	Dry-pressed ceramic
0.25	(0.325, 0.410)	(0.303, 0.359)
0.42	(0.322, 0.400)	(0.301, 0.352)
0.79	(0.319, 0.389)	(0.296, 0.346)
1.10	(0.316, 0.381)	(0.294, 0.339)
1.45	(0.312, 0.372)	(0.289, 0.306)
1.62	(0.305, 0.350)	/

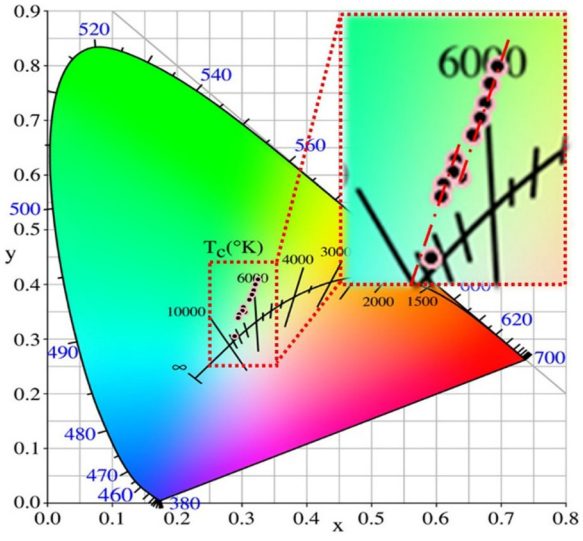

Fig. 12. CIE-1931 chromaticity diagram of the Al_2O_3/YAG: Ce^{3+} ceramic phosphors prepared via conventional dry-pressing and 3D printing. The inset shows the magnified variation tendency.

side surface, demonstrating the excellent structural strength and fine microstructures. This might benefit a lot to the photoluminescence properties, especially as the sample was activated with high power density.

The ceramic slice (φ900 μm × 200 μm) was further encapsulated onto a sapphire substrate using the thermal conductive adhesive, as can be clearly observed in the inset of Fig. 7. The laser light spot was modulated to be the round shape with a diameter of 300 μm using optical lenses. Once the ceramic was irradiated by the laser light (455 nm), strong luminescence was observed. The emission spectrum was recorded in Fig. 7, which was found to be typical spectrum for YAG: Ce^{3+} garnet with a symmetric configuration centered at around 550 nm. The result confirmed that the Ce^{3+} crystalline field surrounding perfectly corresponded to YAG garnet structure.

The power of the laser was tailored by controlling the electrical current and recorded using a dynamometer. The spectra of the converted light as well as the penetrated blue laser were recorded under various laser power ranging from 0.25 to 1.62 W, as presented in Fig. 8(a). The intensity evolution of penetrated light and the converted light was recorded in Fig. 8(b). It can be found that with increasing excitation power, the intensity of the penetrated blue laser increased monotonously, however, the intensity of the converted yellow light deviated from continuous increase and started to drop as the pumping power reached up to 1.62 W, indicating that the conversion efficiency has been beyond saturation. The threshold of the 3D-printed ceramic was evaluated to be about 20.7 W/mm^2 in the present experimental condition. Fig. 9 displays the photographs of the emission light with different power intensity excitation. The emitted yellow light intensity enhanced firstly with increasing pumping power (Fig. 9(a) and (b)), however, further increasing the pumping power (up to 1.62 W) led to a dramatic penetration of blue laser with less yellow light conversion, as shown in Fig. 9(c). The variation in the appearing colors should be intrinsically ascribed to the thermal-induced disturbance of transitions of electrons. As irradiated by laser light with low power density, the thermal effect should be neglectable for the reason that the heat dissipated quickly from the ceramics. Once the power density of irradiation increased beyond a critical point, the thermal effect enhanced remarkably. With the assistance of the intense phonons, more electrons could be successfully excited to the conduction band (CB) and the trapping probability from the CB to the traps increased due to thermal ionization [30], leading to quenching of the luminescence. Furthermore, the accumulated heat would cause more serious heat generation due to stokes shifts of Ce^{3+}. Therefore, the threshold of laser power

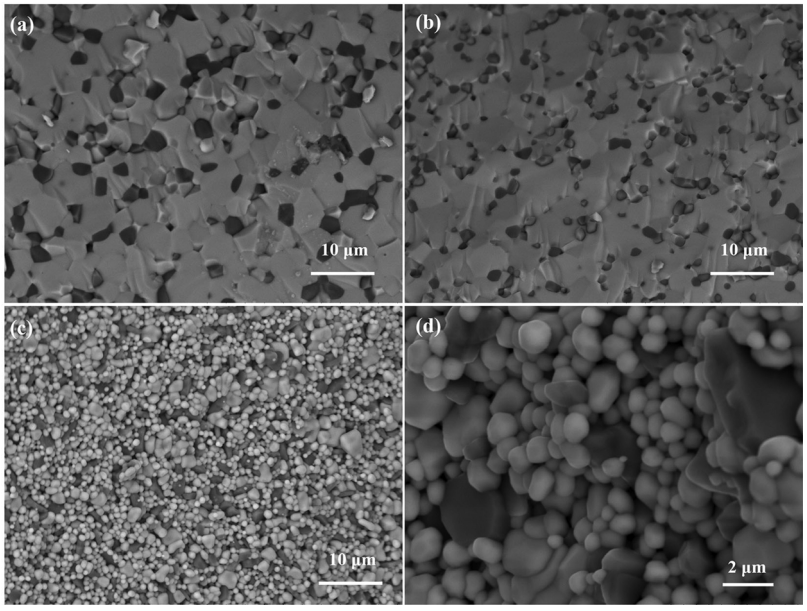

Fig. 13. Microstructure observation of the ceramics after high-flux laser irradiation. Fracture surface of the ceramic prepared via (a) 3D printing and (b) conventional dry-pressing method, respectively; Side view(c) and its magnified image (d) of the dry-pressed columnar ceramic incised from a large ceramic slice via laser cutting.

density as well as luminous flux for the ceramic phosphors should have potentials to be improved by appropriate thermal management.

For comparison, the Al_2O_3/YAG: Ce^{3+} ceramic was prepared at 1720 ℃ via the dry-pressing and vacuum sintering method, as depicted in our previous study [8]. The composition of the powder, including the incorporated sintering additives and the Ce^{3+} concentrations, was totally the same as that used in 3D printing. The obtained ceramic was about 16 mm in diameter and 2 mm in thick. It can be ensured that the ceramic prepared by the conventional method was also provided with a dense microstructure. In order to obtain the same size (φ900 μm × 200 μm), the as prepared ceramic by dry pressing has to be further processed firstly by a line cutting procedure and followed by a laser beam cutting. The line cutting other than double-face polish process was adopted to divide the thick ceramic into thin slices with less material wastage. The new developed laser beam cutting was used to incise the desired tablet from the φ 16 mm-seized slices with accuracy. Then the piece of ceramic was encapsulated onto a sapphire substrate using the same method, the laser spot size was also focused to φ 300 μm in diameter. In this circumstance, the photoluminescence property was characterized for comparison with that of the ceramic prepared via 3D printing, as shown in Fig. 10(a). It can be found that both the penetrated laser light and the converted yellow light showed almost the same variation tendency as that of the ceramic prepared via 3D printing. However, the difference was also conspicuous that the emission intensity began to decline sharply as the excitation power was higher than 1.1 W, much lower than the threshold of 1.45 W of the 3D printed ceramic. In order to figure out the relationship between emission intensity and the pumping power, the plots of the emission intensity versus the excitation power for the ceramic-phosphors prepared via 3D printing and dry-pressing method were exhibited in Fig. 10(b), respectively. Although the dry-pressed ceramic showed a little higher emission intensity at low laser power excitation, the 3D printed ceramic showed higher intensity once the pumping power exceeded 0.25 W. The excitation threshold of the dry-pressed ceramic was calculated to be 15.7 W/mm^2, lower than that of the 3D-printed ceramic. Moreover, the slope of the 3D-printed ceramic was also higher. Fig. 11 showed the photographs of the emission light from Al_2O_3/YAG: Ce^{3+} ceramic prepared via dry-pressing under 1.1 W and 1.45 W laser excitation, respectively. It can be clearly seen that much proportion of the blue laser has penetrated though the ceramic while with less converted light extraction, causing the screen even to burned out as the laser power increased to 1.45 W. Compared with the phenomenon shown in Fig. 9, the 3D-printed ceramic showed much superior light conversion property than that of the dry-pressed ceramic, which was consistent with the luminescence spectra in Fig. 8 and Fig. 10. The conclusion can be confirmed more intuitively from the color coordinates exhibited in Table 1 and those plotted on the CIE-1931 chromaticity diagram, as shown in Fig. 12. For both ceramics, the blue laser light increased more intensely than the converted yellow light, leading to a variation of color coordinates ranging from (0.325, 0.410) to (0.312, 0.372) and (0.303, 0.359) to (0.289, 0.306) for the 3D-printed and dry-pressed ceramics, respectively, under irradiation ranging from 0.25 to 1.45 W. The results indicated that the 3D-printed ceramic exhibited higher light conversion efficiency. This phenomenon should be explained from the viewpoint that differences exist in thermal management property between the 3D-printed and the dry-pressed ceramics according to the analysis in the paragraph above.

The microstructures of the ceramics fabricated via two different methods were observed using SEM, after high-flux laser irradiation, as shown in Fig. 13. The secondary phase of Al_2O_3 dispersed homogenously in the YAG matrix of both ceramics and no cracks or obvious damages were observed in Fig. 13(a) and (b), indicating that the decline of luminescence intensity was not ascribed from the damage of the microstructure of the ceramics. Fig. 13(c) showed the side view of the columnar ceramic incised from the dry-pressed ceramic, the particles were not compactly stacked as the fracture surface shown in Fig. 13(b). During the incision process, a laser beam with a peak laser intensity of 10^{12} W/cm^2 rank was used. The morphological change was mainly due to the laser energy accumulation, according to the Wagner's theory [31]. The laser processed region experienced evolutions including melting, grain boundary diffusion and dislocation diffusion, and finally submicron-sized particles (0.5˜1 μm) appeared in the laser processed region, as displayed in Fig. 13(d). In our viewpoint, the loose microstructure on the columnar side has led to a discretization of thermal conductive behavior and an enhanced phonon scattering on the heterointerface, thus, the heat transport from side face was hindered. On the contrary, SEM of the 3D-printed ceramic observed from the side view (Fig. 6(b)) exhibited compact microstructure because of unconfined grain growth. Moreover, no post processing was adopted to damage the surface benefitting from regulated 3D printing, thus, heat transport happened on all around surfaces more easily. As morphologies or adhesion conditions of upper/down surfaces are kept the same, the cross-section may contribute mostly to the heat transport [32]. Therefore, the 3D-printed ceramic exhibited superior thermal management property and higher threshold of laser flux.

4. Conclusions

A DLP-based 3D printing approach was demonstrated in the present work to obtain ceramic phosphors with fine dimensions (φ = 900 μm) for laser lighting. The composition of the Al_2O_3/YAG: Ce^{3+} ceramic powders was based on our previous study with which high luminous efficiency was guaranteed using the conventional dry-press followed by vacuum sintering method. The mass content of the ceramic suspension for 3D printing was optimized to 77.8%, which contributed to the densification of green bodies and the precision dimensions of the final ceramic product. The spot size of the laser light was focused to 300 μm in diameter for laser lighting characterizations. The luminous intensity was increasing monotonously under the laser irradiation below 1.62 W. However, it began to decline with further increased laser power, due to the thermal ionization in the luminescent center of Ce^{3+}. Both of the dry-pressed and 3D-printed ceramics were comparatively studied. The threshold of laser flux for the 3D-printed ceramic was estimated to be 20.7 W/mm^2, higher than that of the dry-pressed one (15.7 W/mm^2). The difference in the excitation saturation property was ascribed to the microstructure-related thermal management property of the ceramics. Further improving the microstructures of the ceramics via optimizing the suspension compositions, the printing parameters as well as the debinding and sintering procedures would contribute to higher laser-flux-sustaining ceramic phosphors for high-flux laser lighting.

Acknowledgments

This work was supported by National Key R&D Program of China (No. 2018YFC0308100) and Science Foundation for Youth Scholar of State Key Laboratory of High Performance Ceramics and Superfine Microstructures (No. SKL201802).

References

[1] X. Zhang, L. Huang, F. Pan, M. Wu, J. Wang, Y. Chen, Q. Su, Highly thermally stable single-component white-emitting silicate glass for organic-resin-Free white-light-emitting diodes, ACS Appl. Mater. Interfaces 6 (2014) 2709–2717.

[2] L. Wang, R.J. Xie, Y. Li, X. Wang, C.G. Ma, D. Luo, T. Takeda, Y.T. Tsai, R.S. Liu, N. Hirosaki, $Ca_{1-x}Li_xAl_{1-x}Si_{1+x}N_3:Eu^{2+}$ solid solutions as broadband, color-tunable and thermally robust red phosphors for superior color rendition white light-emitting diodes, Light Sci. Appl. 5 (2016) e16155.

[3] X.J. Zhang, S. Si, J. Yu, Z. Wang, R. Zhang, B. Lei, Y. Liu, J. Zhuang, C. Hu, Y. Cho, R. Xie, H. Zhang, Z. Tian, J. Wang, Improving the luminous efficacy and resistance to blue laser irradiation of phosphor-in-Glass based solid state laser lighting through employing dual-functional sapphire plate, J. Mater. Chem. C 7 (2019) 354–361.

[4] C. Cozzan, G. Lheureux, N. O'Dea, E.E. Levin, J. Graser, T.D. Sparks, S. Nakamura, S.P. DenBaars, C. Weisbuch, R. Seshadri, Stable, heat-conducting phosphor composites for high-power laser lighting, ACS Appl. Mater. Interfaces 10 (2018) 5673–5681.

[5] S. Hu, C. Lu, G. Zhou, X. Liu, X. Qin, G. Liu, S. Wang, Z. Xu, Y.A.G. Transparent, Ce ceramics for WLEDs with high CRI: Ce^{3+}: concentration and sample thickness effects, Ceram. Int. 42 (2016) 6935–6941.
[6] S. Liu, P. Sun, Y. Liu, T. Zhou, S. Li, R.-J. Xie, X. Xu, R. Dong, J. Jiang, H. Jiang, Warm white light with a high color rendering index from a single $Gd_3Al_4GaO_{12}:Ce^{3+}$ transparent ceramic for high-power LEDs and LDs, ACS Appl. Mater. Interfaces (2018), https://doi.org/10.1021/acsami.8b18103.
[7] Y. Tang, S. Zhou, C. Chen, X. Yi, Y. Feng, H. Lin, S. Zhang, Composite phase ceramic phosphor of Al_2O_3-Ce:YAG for high efficiency light emitting, Opt. Express 23 (2015) 17923–17928.
[8] S. Hu, Y. Zhang, Z. Wang, G. Zhou, Z. Xue, H. Zhang, S. Wang, Phase composition, microstructure and luminescent property evolutions in "Light-scattering Enhanced" Al_2O_3-$Y_3Al_5O_{12}$: Ce^{3+} ceramic phosphors, J. Eur. Ceram. Soc. 38 (2018) 3268–3278.
[9] Y.H. Song, E.K. Ji, B.W. Jeong, M.K. Jung, E.Y. Kim, C.W. Lee, D.H. Yoon, Design of laser-driven high-efficiency Al_2O_3/YAG:Ce^{3+} ceramic converter for automotive lighting: fabrication, luminous emittance, and tunable color space, Dyes Pigm. 139 (2017) 688–692.
[10] S. Li, Q. Zhu, D. Tang, X. Liu, G. Ouyang, L. Cao, N. Hirosaki, T. Nishimura, Z. Huang, R.J. Xie, Al_2O_3-YAG:Ce composite phosphor ceramic: a thermally robust and efficient color converter for solid state laser lighting, J. Mater. Chem. C 4 (2016) 8648–8654.
[11] Y.H. Song, S.B. Kwon, M.K. Jung, W.K. Park, J.H. Yoo, C.W. Lee, B.K. Kang, W.S. Yang, D.H. Yoon, Fabrication design for a high-quality laser diode-based ceramic converter for a laser headlamp application, Ceram. Int. 44 (2018) 1182–1186.
[12] F. Tang, Y. Cao, J. Huang, W. Guo, H. Liu, Q. Huang, W. Wang, Multilayer YAG/Re:YAG/YAG laser ceramic prepared by tape casting and vacuum sintering method, J. Eur. Ceram. Soc. 32 (2012) 3995–4002.
[13] Y. Sun, X. Qin, G. Zhou, H. Zhang, X. Peng, S. Wang, Gelcasting and reactive sintering of sheet-like YAG transparent ceramics, J. Alloys Compd. 652 (2015) 250–253.
[14] Y.K. Kshetri, B. Joshi, S.W. Lee, Intense visible upconversion emission in transparent (Ho^{3+}, Er^{3+})-alpha-Sialon ceramics under 980 nm laser excitation, J. Eur. Ceram. Soc. 36 (2016) 4215–4224.
[15] X. Chen, H. Qin, X. Wang, C. Yang, J. Jiang, H. Jiang, Sintering and characterisation of $Gd_3Al_3Ga_2O_{12}$/$Y_3Al_5O_{12}$ layered composite scintillation ceramic, J. Eur. Ceram. Soc. 36 (2016) 2587–2591.
[16] J. Xu, J. Wang, Y. Gong, X. Ruan, Z. Liu, B. Hu, B. Liu, H. Li, X. Wang, B. Du, Investigation of an LuAG:Ce translucent ceramic synthesized via spark plasma sintering: towards a facile synthetic route, robust thermal performance, and high-power solid state laser lighting, J. Eur. Ceram. Soc. 38 (2018) 343–347.
[17] G.N. Levy, R. Schindel, J.P. Kruth, Rapid manufacturing and rapid tooling with layer manufacturing (LM) technologies, state of the art and future perspectives, CIRP Ann. Manuf. Technol. 52 (2003) 589–609.
[18] J. Deckers, J. Vleugels, J.P. Kruthl, Additive manufacturing of ceramics: a review, J. Ceram. Sci. Technol. 5 (2014) 245–260.
[19] D.H. Kim, J. Lee, J. Bae, S. Park, J. Choi, J.H. Lee, E. Kim, Mechanical analysis of Ceramic/Polymer composite with mesh-type lightweight design using binder-jet 3D printing, Materials 11 (2018) 1941.
[20] C. Yang, X. Wang, B. Ma, H. Zhu, Z. Huan, N. Ma, C. Wu, J. Chang, 3D-printed bioactive Ca_3SiO_5 bone cement scaffolds with nano surface structure for bone regeneration, ACS Appl. Mater. Interfaces 9 (2017) 5757–5767.
[21] H. Ma, C. Feng, J. Chang, C. Wu, 3D-printed bioceramic scaffolds: from bone tissue engineering to tumor therapy, Acta Biomater. 79 (2018) 37–59.
[22] S. Li, W. Duan, T. Zhao, W. Han, L. Wang, R. Dou, G. Wang, The fabrication of SiBCN ceramic components from preceramic polymers by digital light processing (DLP) 3D printing technology, J. Eur. Ceram. Soc. 38 (2018) 4597–4603.
[23] G.A. Dosovitskiy, P.V. Karpyuk, P.V. Evdokimov, D.E. Kuznetsova, V.A. Mechinsky, A.E. Borisevich, A.A. Fedorov, V.I. Putlayev, A.E. Dosovitskiy, M.V. Korjik, First 3D-printed complex inorganic polycrystalline scintillator, Crystengcomm 19 (2017) 4260–4264.
[24] Y. Ben, L. Zhang, S. Wei, T. Zhou, Z. Li, H. Yang, C. Wong, H. Chen, Improved forming performance of β-TCP powders by doping silica for 3D ceramic printing, J. Mater. Sci. Mater. Electron. 28 (2017) 5391–5397.
[25] X. Wang, M. Jiang, Z. Zhou, J. Gou, D. Hui, 3D printing of polymer matrix composites: a review and prospective, Compos. Pt. B Eng. 110 (2017) 442–458.
[26] F. Frascella, G. Gonzalez, P. Bosch, A. Angelini, A. Chiappone, M. Sangermano, C.F. Pirri, I. Roppolo, 3D printed photoluminescent polymeric waveguides, ACS Appl. Mater. Interfaces 10 (2018) 39319–39326.
[27] T. Ishikawa, S. Sakata, A. Mitani, Durable, ultraluminous structure for incandescent, high-power White-LED, Int. J. Appl. Ceram. Technol. 3 (2006) 144–149.
[28] Q. Sai, Z. Zhao, C. Xia, X. Xu, F. Wu, J. Di, L. Wang, Ce-doped Al_2O_3-YAG eutectic and its application for white LEDs, Opt. Mater. 35 (2013) 2155–2159.
[29] H. Su, Y. Nie, H. Yang, D. Tang, K. Chen, T. Zhang, Improving the thermal stability of phosphor in a white light-emitting diode (LED) by glass-ceramics: effect of Al_2O_3 dopant, J. Eur. Ceram. Soc. 38 (2018) 2005–2009.
[30] J. Ueda, P. Dorenbos, A.J.J. Bos, A. Meijerink, S. Tanabe, Insight into the thermal quenching mechanism for $Y_3Al_5O_{12}:Ce^{3+}$ through thermo luminescence excitation spectroscopy, J. Phys. Chem. C 119 (2005) 25003–25008.
[31] C. Wagner, The theory of the warm-up process, Zeitschrift Fur Physikalische Chemie-Abteilung B-Chemie Der Elementarprozesse Aufbau Der Materie 21 (1933) 25–41.
[32] G.H. Liu, Z.Z. Zhou, Y. Shi, Q. Liu, J.Q. Wan, Y.B. Pan, Ce:YAG transparent ceramics for applications of high power LEDs: thickness effects and high temperature performance, Mater. Lett. 139 (2015) 480–482.